JOC The Journal of Organic Chemistry

Article

pubs.acs.org/joc

Memory Effects in Carbocation Rearrangements: Structural and Dynamic Study of the Norborn-2-en-7-ylmethyl-X Solvolysis Case

Giovanni Ghigo,* Andrea Maranzana, and Glauco Tonachini

Dipartimento di Chimica, Università di Torino, V. Giuria 7, I-10125 Torino, Italy

Supporting Information

ABSTRACT: The solvolysis of two diastereomers may give the same two products, but in different ratios, notwithstanding the fact that the two reaction pathways share an apparently identical intermediate carbocation. This has been dubbed the "*memory effect*", since the initial carbocation seems to "remember" its origin when undergoing further evolutions through multistep rearrangements. This puzzling result was studied theoretically for the case of the solvolysis of norborn-2-en-7-ylmethyl-X systems by defining the reaction potential energy surface (PES) and then carrying out a dynamical study. The PES shows that upon X^- loss, multiphase rearrangements concertedly yield the two stablest carbocations, **G** and **L**. These carbocations are connected by a transition structure. The carbocation intermediates proposed in the literature do not correspond to any stationary point. The preference for the rearrangement to **G** or **L** (the *memory effect*) is determined by structural and stereoelectronic effects: the competitive interaction between an empty p orbital with a σ orbital or a p/π orbital is guided by geometrical aspects present in the starting carbocations. The dynamical study shows that (1) **G** and **L** do not interconvert and (2) the evolving system can switch from one pathway to the other to different extents, thus determining a more or less pronounced memory loss (the *leakage*).

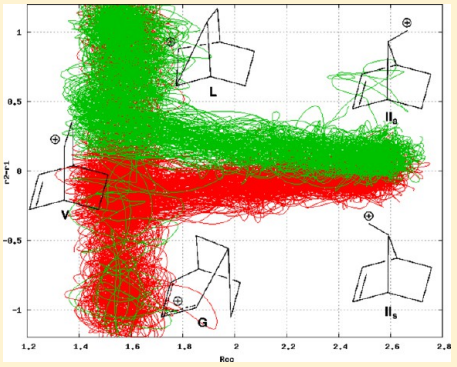

INTRODUCTION

The *memory effect*[1] involves stereochemical control of a reaction center operated by a different center localized on the same molecule. The most known case is the neighboring-group effect, which leads to the configuration being maintained in some solvolyses (Scheme 1 shows two examples[2]).

Scheme 1. *Memory Effect* Due to the Neighboring-Group Effect

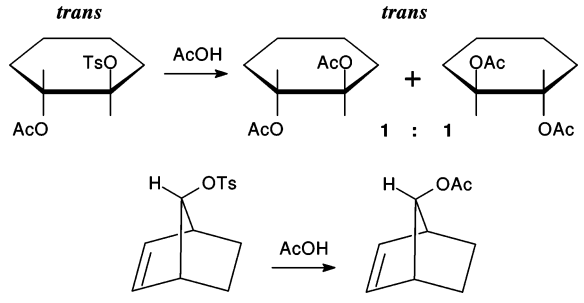

In some cases, such control can be exercised by a more remote center. In particular, the *memory effect* has been invoked in the multiple rearrangement of carbocations when the two stereoisomers of the precursor rearrange to give different products despite the apparent existence of some common intermediate along the reaction pathway. This case is illustrated by Scheme 2, which shows the solvolysis with rearrangement of **R**–**X** that takes place through carbocation intermediates $\mathbf{R}^+$ and $\mathbf{M}^+$.

Scheme 2. *Memory Effect* in the Multiple Carbocation Rearrangement

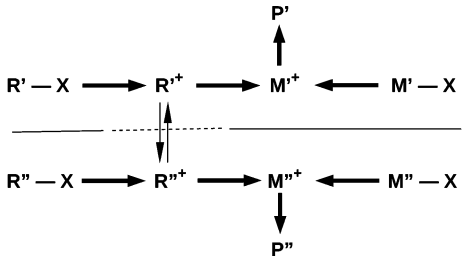

Here we can see that solvolysis of the stereoisomer **R′**–**X** mainly yields product **P′** while that of the stereoisomer **R″**–**X** mainly yields product **P″**. The presence of a memory effect is evidenced by the fact that intermediates $\mathbf{R''}^+$ and $\mathbf{R'}^+$ are expected to interconvert easily because they are linked by a simple conformational relation (in contrast to being just the same structure, which would leave the effect unexplained). The picture is completed by the observation that the solvolysis of **M′**–**X** yields exclusively product **P′** while the solvolysis of **M″**–**X** yields exclusively product **P″**. Intermediates $\mathbf{M'}^+$ and $\mathbf{M''}^+$ are structural isomers (not just stereoisomers), and they do not interconvert. Their formation from **M′**–**X** and **M″**–**X** involves a rearrangement, often with some neighboring-group effect.

Received: May 31, 2013
Published: August 20, 2013

dx.doi.org/10.1021/jo401188e | J. Org. Chem. 2013, 78, 9041–9050

Scheme 3. *Memory Effect* As Proposed in the Literature

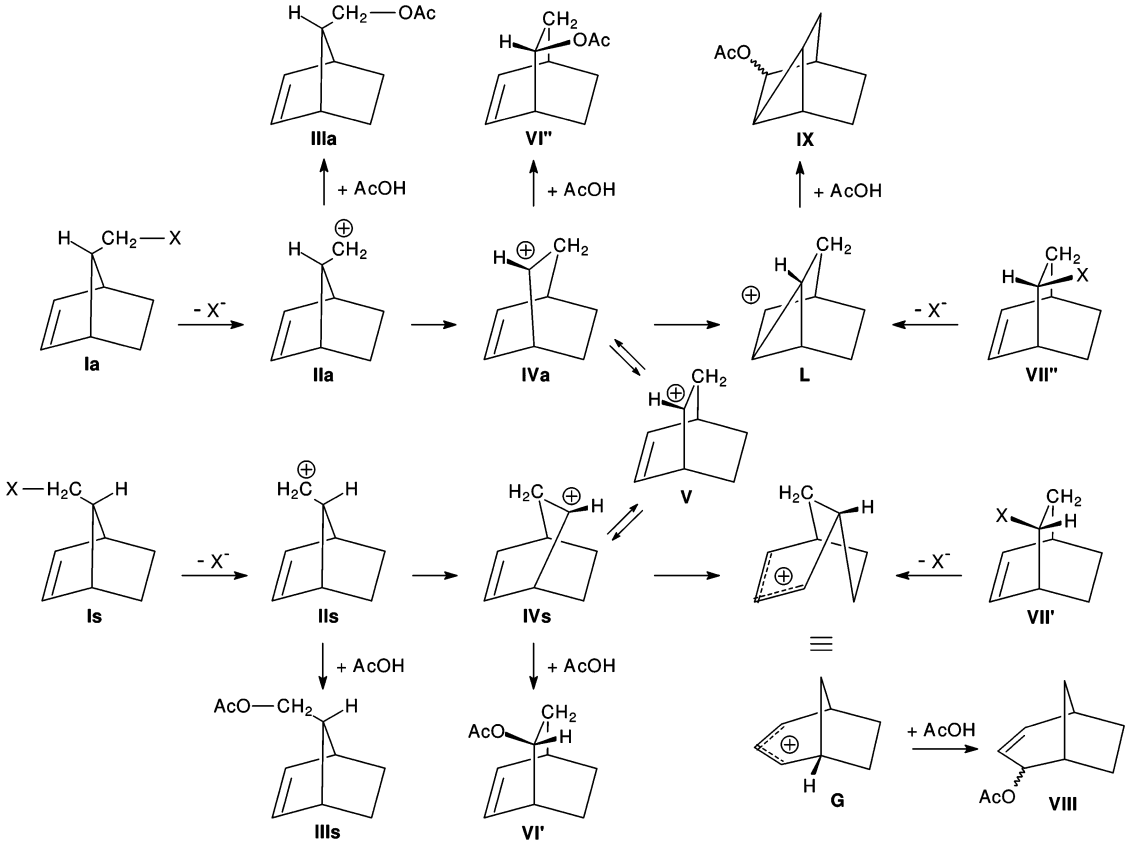

Table 1. Yield Ratios and Excesses of the Acetates of Cations G and L in the Solvolysis of Norborn-2-en-7-ylmethyl Derivatives I_s and I_a

	syn (I_s)		*anti* (I_a)	
leaving group (X)	G/L	% excess G[a]	L/G	% excess L[b]
N_2 (from NH_2)	3–5	45–65	30–70	94–97
ONs	3–5	47–64	3.5–4.5	56–64
Br	2–4	33–64	42–45	82–96

[a]% excess G = 100% × (G − L)/(G + L). [b]% excess L = 100% × (L − G)/(L + G).

Table 2. Relative Energies ΔE (ΔE_{el} + ΔZPE) in the Solvolysis of Norborn-2-en-7-ylmethyldiazonium

	ΔE (kcal mol^{-1})		
structure	B3LYP	mPW1PW91	BB1K
I_s–NN^+	0.0	0.0	0.0
TS to II_s + N_2	5.0	8.2	8.0
TS to II_s^{NC} + N_2	9.3	11.8	11.3
I_a–NN^+	2.2	2.1	2.0
TS to II_a + N_2	7.3	10.5	10.2

This kind of stereochemical control was first observed as early as 1961 by Silver[3] and a year later by Berson and co-workers,[4] who dubbed it the *memory effect*.[1] Other studies by Berson and co-workers in the 1960s[5] and by Collins and co-workers in the early 1970s[6] followed the initial reports. Despite the great amount of experimental work, the causes of the *memory effect* are not fully understood. Therefore, we have undertaken the study of this stereochemical control by theoretical methods. We

Scheme 4. Generation of Carbocations from the Solvolysis of Norborn-2-en-7-ylmethyldiazonium

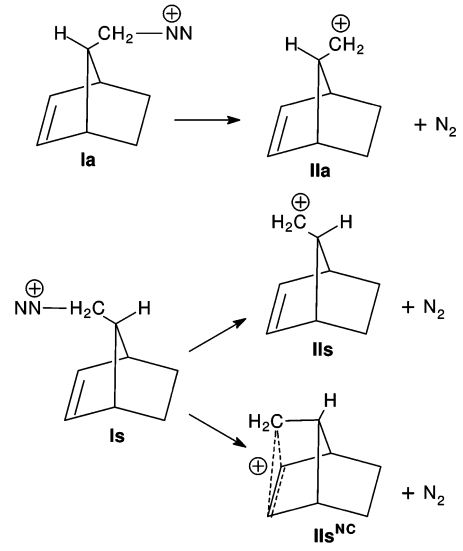

have chosen, among several cases, the norborn-2-en-7-ylmethyl cation derived from acetolysis of different **X**-substituted norborn-2-en-7-ylmethyl systems, which is the most famous case.[7] Starting from its *syn* (I_s) and *anti* (I_a) diastereomers (Scheme 3), in addition to small amounts of the products of the simple solvolysis (III_s and III_a) they also observed the formation of different amounts of the two distinct products belonging to the so-called Goering series[8] (**VIII** from carbocation **G**) and Le Bel series[9] (**IX** from carbocation **L**). In his paper, Berson suggested

dx.doi.org/10.1021/jo401188e | J. Org. Chem. 2013, 78, 9041–9050

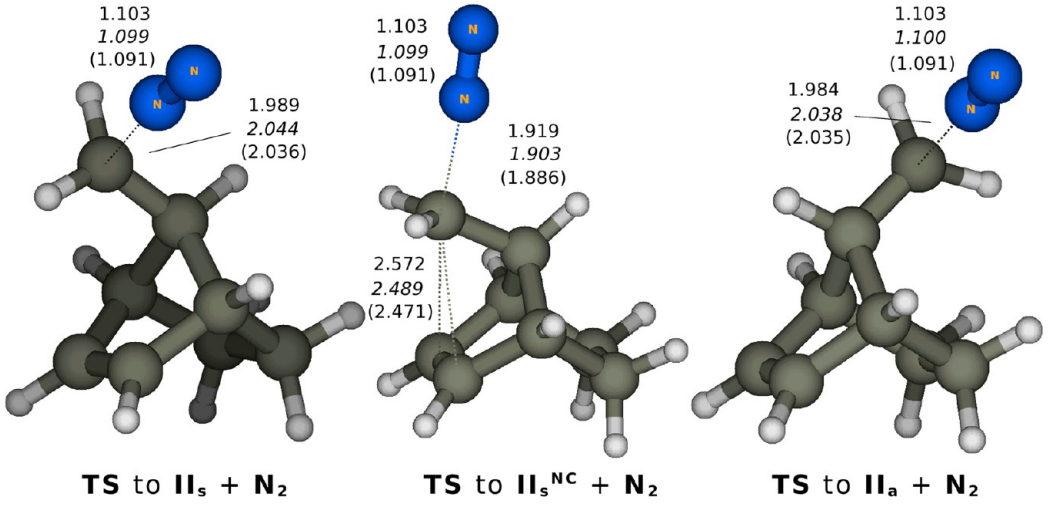

Figure 1. Transition structures for the solvolysis of norborn-2-en-7-ylmethyldiazonium. Values in plain text, B3LYP; values in italics, mPW1PW91; values in parentheses, BB1K.

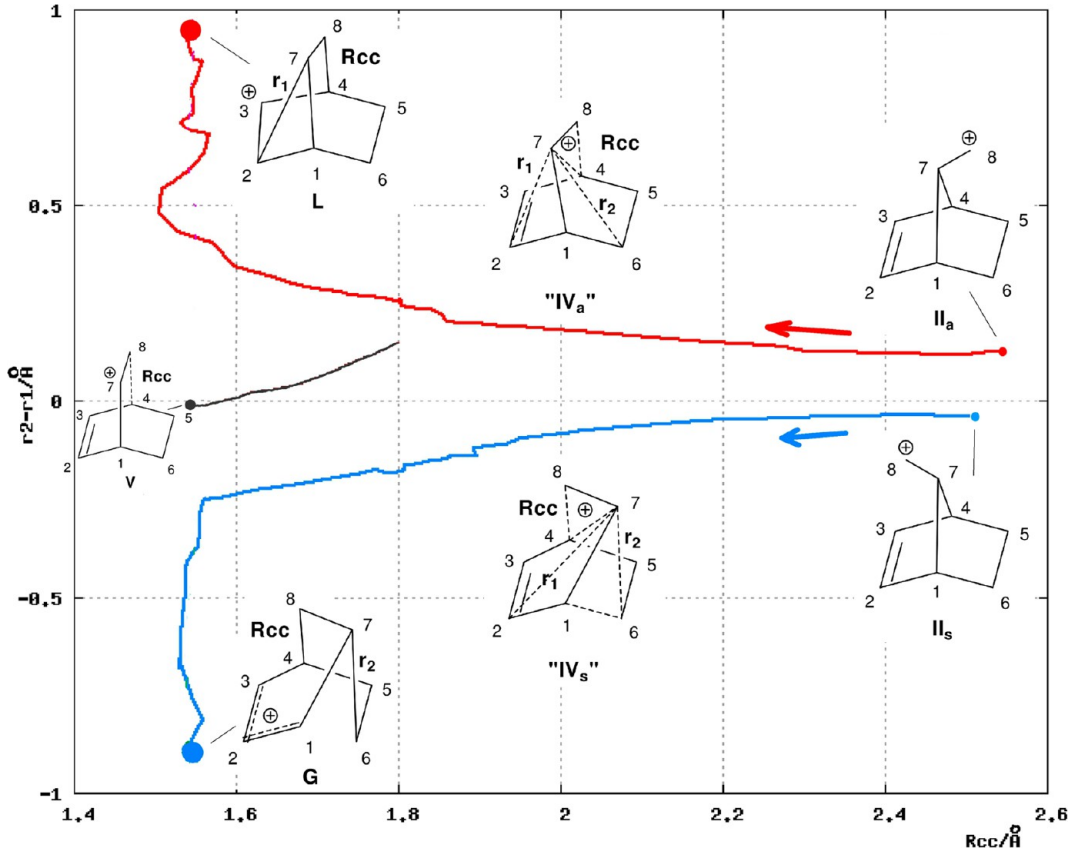

Figure 2. More O'Ferrall–Jencks diagram of the B3LYP IRCs for the rearrangement of cations $\mathbf{II}_s$ (blue line) and $\mathbf{II}_a$ (red line) and the ridge from **TS V** (gray line). The positions of cations **V**, **G**, and **L** are indicated by dots. R_{CC} is the C^4-C^8 distance; r_1 is the C^7-C^2 distance; and r_2 is the C^7-C^6 distance. Values are in Å.

that after the ionic detachment of the leaving groups, the two norborn-2-en-7-ylmethyl carbocations $\mathbf{II}_s$ and $\mathbf{II}_a$ can rearrange to cations $\mathbf{IV}_s$ and $\mathbf{IV}_a$ before the capture of the solvent. These two carbocations could yield the corresponding products of solvent capture, **VI′** and **VI″** (which are indeed found in very small amounts), or give rise to a second rearrangement leading, respectively, to the final products from cation **G** (from $\mathbf{I}_s$) and cation **L** (from $\mathbf{I}_a$). The observation that solvolysis of the *syn* isomer $\mathbf{I}_s$ mainly leads to product **VIII** (from **G**) while that of the *anti* isomer $\mathbf{I}_a$ mainly leads to product **IX** (from **L**) through cations $\mathbf{IV}_s$ and $\mathbf{IV}_a$, respectively, which are just two conformers of the same carbocation, suggests the existence of some sort of "*memory effect*" that causes the two cations to "remember" the cations from which they came. Indeed, in the solvolysis of $\mathbf{I}_a$ small amount of product **IX** was also found, and conversely, in the solvolysis of $\mathbf{I}_a$ a small amount of product **VIII** was also

dx.doi.org/10.1021/jo401188e | J. Org. Chem. 2013, 78, 9041–9050

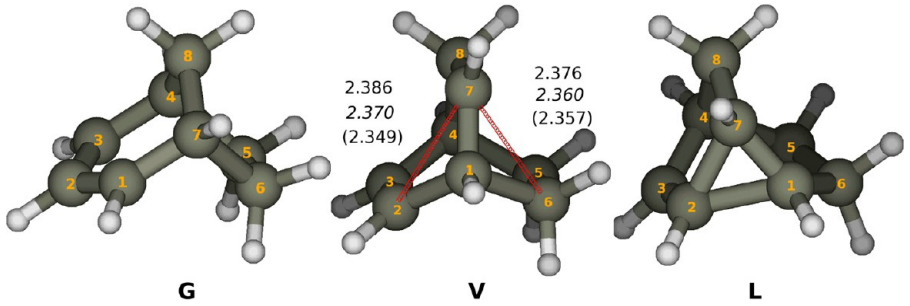

Figure 3. Structures of cations **G** and **L** and TS **V**. Plain text, B3LYP; italics, mPW1PW91; in parentheses, BB1K.

Table 3. Relative Energies ΔE (ΔE_{el} + ΔZPE) in the Rearrangements of Carbocations II_s and II_a

	ΔE (kcal mol^{-1})		
structure	B3LYP	mPW1PW91	BB1K
II_s	44.2	44.2	42.9
II_s^{NC}	31.5	24.8	20.0
II_a	47.3	47.3	46.1
V	17.6	16.8	16.8
L	7.1	3.6	1.7
G	0.0	0.0	0.0

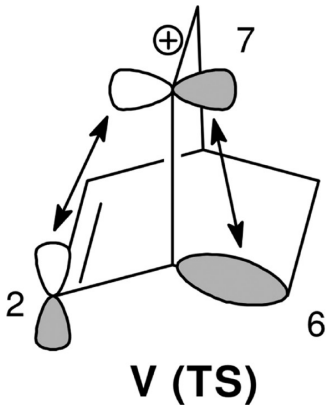

Figure 4. Orbital interactions in the carbocationic structure **V**.

found. This suggested the occurrence of some equilibration between the two cations IV_s and IV_a through a transition structure **V** or possibly the existence of an intermediate structure **V** that connects cations IV_s and IV_a. This equilibration determinates a partial loss of the *memory effect*, a phenomenon known as *leakage*.

Despite the elegance of Scheme 3, a full comprehension of this phenomenon was not achieved: the experimental findings (isotope labeling and a substantial lack of ion couples and solvent effects) demonstrated only that "*memory therefore must be preserved in processes passing through carbonium ions, not in bimolecular nucleophilic reactions*".[5d] A role for "asymmetric ionic solvation" was also excluded by Berson.[5d] Collins[6c] proposed this role again, but his experiments were performed on completely different systems. Another fact complicates the picture: solvolysis of the two tosylates of 2-bicyclo[2.2.2]oct-5-enyl (**VII′** and **VII″**) yields only the rearrangement products, acetate **VIII** of cation **G** derived from **VII′** and acetate **IX** of cation **L** derived from **VII″**.[5a] This result confirms that the equilibration (if any) is not between cations **G** and **L**. However, in view of the fact that the heterolysis of the two tosylates must form cations IV_s and IV_a, it is hard to explain why there is not a partial loss of the *memory effect* that would again result in the formation of the acetate of cation **G** from **VII″** and the acetate of cation **L** from **VII′**. In the experiments,[5a] several leaving groups were used, and in all cases, the *memory effect* with some *leakage* was observed. Table 1 collects the different cases. We stress that

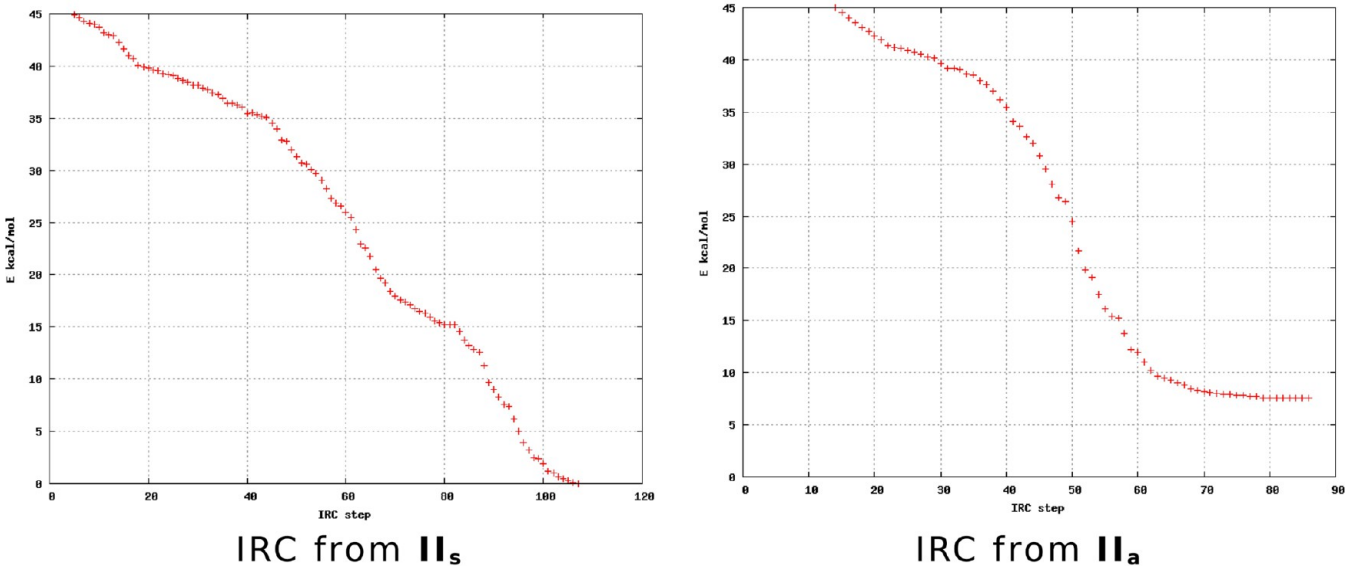

Figure 5. Energy profiles along the B3LYP IRCs for the rearrangement of cations II_s (left) and II_a (right).

dx.doi.org/10.1021/jo401188e | *J. Org. Chem.* 2013, 78, 9041−9050

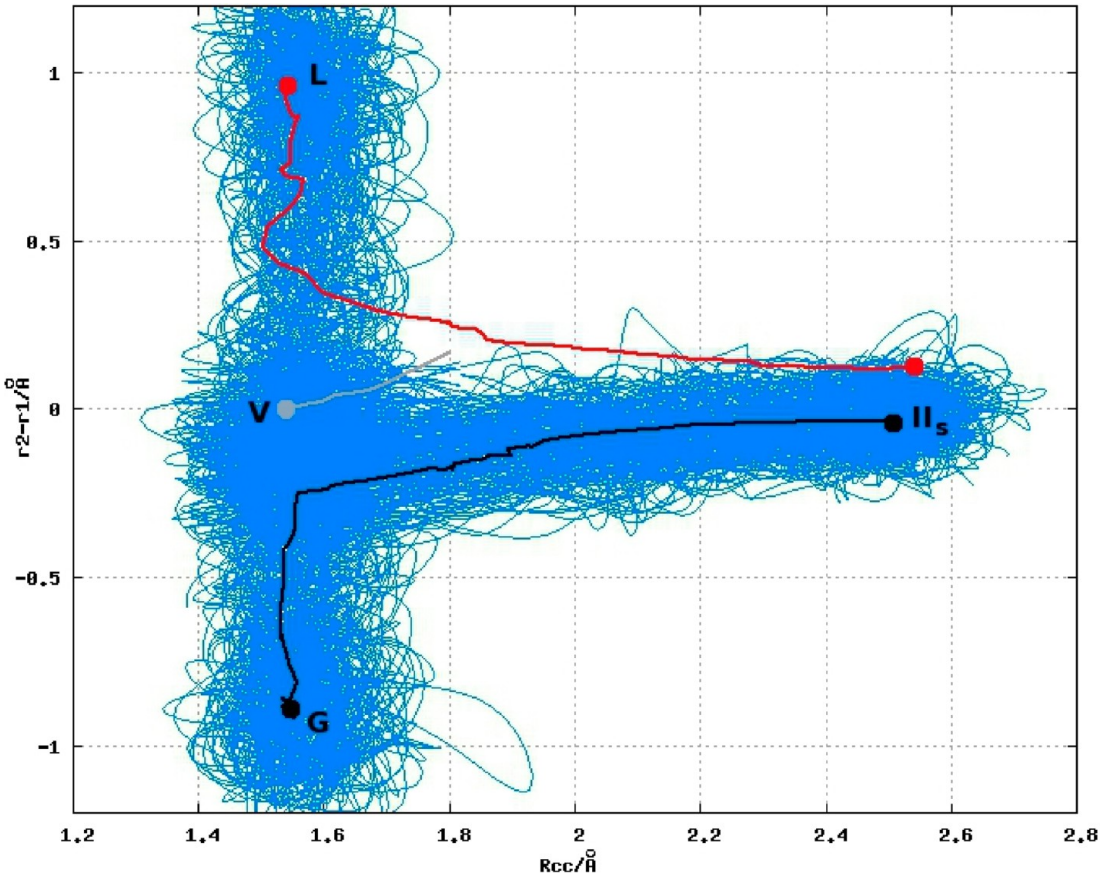

Figure 6. More O'Ferrall–Jencks diagram showing trajectories relevant to the rearrangement of cation $\mathbf{II}_s$. For definitions of R_{CC}, r_1, and r_2, see the Figure 2 caption.

without *leakage*, solvolysis of the *syn* isomer should yield only the acetate of **G** and solvolysis of the *anti* isomer only the acetate of **L**. We can observe that solvolysis of the *syn* isomer presents quite an extended *leakage*, while solvolysis of the *anti* isomer presents a quite extended *memory* of the starting molecule.

The nature of the leaving group changes the relative yields, but the presence of the *memory effect* and the different extents of *leakage* for the *syn* and *anti* isomers are unchanged. In the main part of our study, the leaving groups and solvent molecules were not present. This prevented us from observing the effect of the leaving groups on the yields and the alternative pathways such as deprotonation (which were, however, experimentally[5] found to be negligible). However, the experiments[5] proved that the rearrangements involve only carbonium ions, that ion couples are excluded, and most importantly, that no products of counterion recapture were isolated.

Our goal was to unravel the most important factors that lead to the *memory effect* and the *leakage* phenomenon. Therefore, our computational study was mainly focused on the free carbocations starting from the cations $\mathbf{II}_s$ and $\mathbf{II}_a$ after a preliminary analysis of their generation.

RESULTS AND DISCUSSION

The formation of cations $\mathbf{II}_s$ and $\mathbf{II}_a$ is a consequence of heterolysis of the **C–X** bonds in $\mathbf{I}_s$ and $\mathbf{I}_a$, respectively, induced by the ionizing solvent. In the former, heterolysis can also generate the nonclassical carbocation $\mathbf{II}_s^{NC}$ (Scheme 4). Studies of the heterolysis of the diazonium derivatives[10] (**X** = N_2^+; Table 2 and Figure 1) showed that the formation of $\mathbf{II}_s^{NC}$ is negligible with respect to the formation of $\mathbf{II}_s$ (by all three methods, the yield was estimated to be <0.5% at room temperature).

On the basis of the experimental evidence, we assumed that once the transition structure (TS) is overcome, **X** moves apart and leaves the reacting system. Therefore, we could proceed with our main intent, which was to confirm the existence on the potential energy surface (PES) of the carbocation intermediates shown in Scheme 3. The PES is illustrated by the More O'Ferrall–Jencks plot (Figure 2), where R_{CC} is the distance between $\mathbf{C}^4$ and $\mathbf{C}^8$, r_1 is the distance between $\mathbf{C}^7$ and $\mathbf{C}^2$, and r_2 is the distance between $\mathbf{C}^7$ and $\mathbf{C}^6$ (although important, the $\mathbf{C}^4$–$\mathbf{C}^7$ distance is not shown in the bidimensional plot). On the right side of the plot (at long R_{CC}, $r_2 - r_1$ close to zero, and short $\mathbf{C}^4$–$\mathbf{C}^7$), we find cations $\mathbf{II}_s$ and $\mathbf{II}_a$, while in the left side (short R_{CC} and long $\mathbf{C}^4$–$\mathbf{C}^7$), we find cations **L** (at $r_2 - r_1 \approx 0.9$) and **G** (at $r_2 - r_1 \approx -0.9$).

Cation **G** (large blue dot in Figure 2 left; structure in Figure 3) is the most stable structure, since it contains a 1,3-disubstituted allyl system. Therefore, it has been used as the energy reference in Table 3. **G** and **L** (a secondary carbocation stabilized by a fused three-carbon ring, with ΔE = 2–7 kcal mol^{-1}; large red dot in Figure 2left, structure in Figure 3) were found to be real intermediates. Cation $\mathbf{II}_s^{NC}$ is the nonclassical carbocation originating from the alternative solvolysis of $\mathbf{I}_s$. Because its formation was negligible (see Table 2), further evolutions were not analyzed.

By contrast, cations $\mathbf{IV}_s$ and $\mathbf{IV}_a$ do not exist as stationary points on the PES. Moreover, the structures $\mathbf{II}_s$ and $\mathbf{II}_a$ (the primary

dx.doi.org/10.1021/jo401188e | J. Org. Chem. 2013, 78, 9041–9050

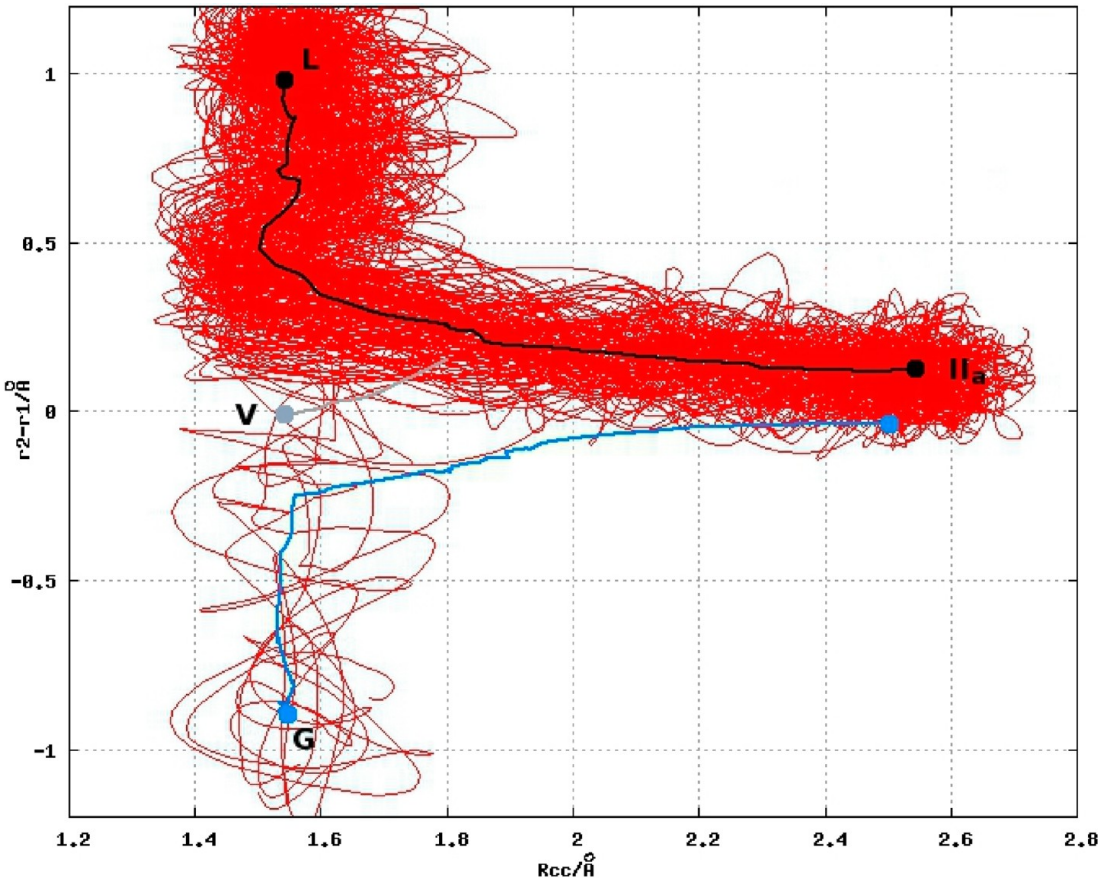

Figure 7. More O'Ferrall–Jencks diagram showing trajectories relevant to rearrangement of cation $\mathbf{II}_a$. For definitions of R_{CC}, r_1, and r_2, see the Figure 2 caption.

carbocation structures; Figure 2 right) and **V** (a secondary carbocation structure) were indeed found to be transition structures and not stable cations. In particular, TS **V** (17 kcal mol^{-1}; gray dot in Figure 2 left, structure in Figure 3) directly connects cations **G** and **L**. The gray line in Figure 2 is the ridge that originates from **V** and "separates" the **G** region from the **L** region. From a stereochemical point of view, we can see that the empty p orbital on $\mathbf{C}^7$ gives two competing stabilizing orbital interactions (Figure 4): one with the σ orbital of the $\mathbf{C}^1$–$\mathbf{C}^6$ bond (leading to cation **G**) and the other with the p/π orbital on $\mathbf{C}^2$ (leading to cation **L**). In this almost symmetrical structure (r_1 = 2.386 Å, r_2 = 2.376 Å) there is a balance between the two interactions that "pull" $\mathbf{C}^7$ toward $\mathbf{C}^6$ or $\mathbf{C}^2$, respectively, in TS **V**.

In $\mathbf{II}_s$ (44 kcal mol^{-1} with respect to **G**) and $\mathbf{II}_a$ (46–47 kcal mol^{-1}) the vibrational mode with imaginary frequency corresponds to stretching of the $\mathbf{C}^4$–$\mathbf{C}^7$ (or $\mathbf{C}^1$–$\mathbf{C}^7$) bond and oscillation of $\mathbf{C}^8$ toward $\mathbf{C}^4$ (or $\mathbf{C}^1$). The energy profiles along the intrinsic reaction coordinates (IRCs) (Figure 5), corresponding to the blue and red lines starting from the right side in Figure 2, show that these atom displacements correspond to the "first rearrangement" of cations $\mathbf{II}_s$ and $\mathbf{II}_a$ that should yield the more stable secondary carbocations $\mathbf{IV}_s$ and $\mathbf{IV}_a$. These structures, however, do not correspond to stationary points on the PES (they are neither minima nor transition structures), which means that the chemical process does not stop in a single step. While the $\mathbf{C}^8$–$\mathbf{C}^4$ bond completes its formation (R_{CC} gets below 1.6 Å), carbon $\mathbf{C}^7$ bends toward $\mathbf{C}^6$ (if coming from $\mathbf{II}_s$) or toward $\mathbf{C}^2$ (if coming from $\mathbf{II}_a$), giving rise to the "second rearrangement". A "slight shoulder",[11a] which appears in the energy profile of the IRC from $\mathbf{II}_s$ at around the 80th point (Figure 5 left), hints at a structure as carbocation $\mathbf{IV}_s$. However, this structure cannot be considered as a proper intermediate because it does not correspond to an energy minimum. By contrast, the energy profile for the IRC from $\mathbf{II}_a$ (Figure 5 right) does not suggest the existence of any carbocation intermediate. Therefore, each reaction path follows a curve (left side in Figure 2) that finally yields either cation **G** or **L**, describing a "*two-stage*" asynchronous concerted process.[11] The More O'Ferrall–Jencks plot clearly shows the nature of the *memory effect*: in each rearrangement, cation $\mathbf{IV}_s$ or $\mathbf{IV}_a$ is not present on the PES as a stationary point, which means that the structure of the starting carbocation determines the final product. In fact, in cation $\mathbf{II}_s$, the distance between $\mathbf{C}^7$ and $\mathbf{C}^6$ (r_2) is already shorter than the distance between $\mathbf{C}^7$ and $\mathbf{C}^2$ (r_1). Therefore, when the rearrangement starts, $\mathbf{C}^7$ is attracted by the $\mathbf{C}^6$ center ($r_2 - r_1$ becomes more negative) because the orbital interaction between incipient empty p orbital on $\mathbf{C}^7$ and the σ orbital of the $\mathbf{C}^1$–$\mathbf{C}^6$ bond prevails. Consequently, the two rearrangements take place concertedly (though asynchronously) to finally yield cation **G**. The same structural guidance occurs for cation $\mathbf{II}_a$, where the shorter distance between $\mathbf{C}^7$ and $\mathbf{C}^2$ (r_1 and $r_2 - r_1$ positive) dictates a concerted rearrangement to give cation **L**. In this case, it is the interaction between the incipient empty p orbital on $\mathbf{C}^7$ and the p/π orbital on $\mathbf{C}^2$ that prevails. In both cases, the rearrangements are quite exothermic (by more than 40 kcal mol^{-1}). Therefore, the PES can be described as two valleys originating from $\mathbf{II}_s$ and $\mathbf{II}_a$ that are

dx.doi.org/10.1021/jo401188e | J. Org. Chem. 2013, 78, 9041–9050

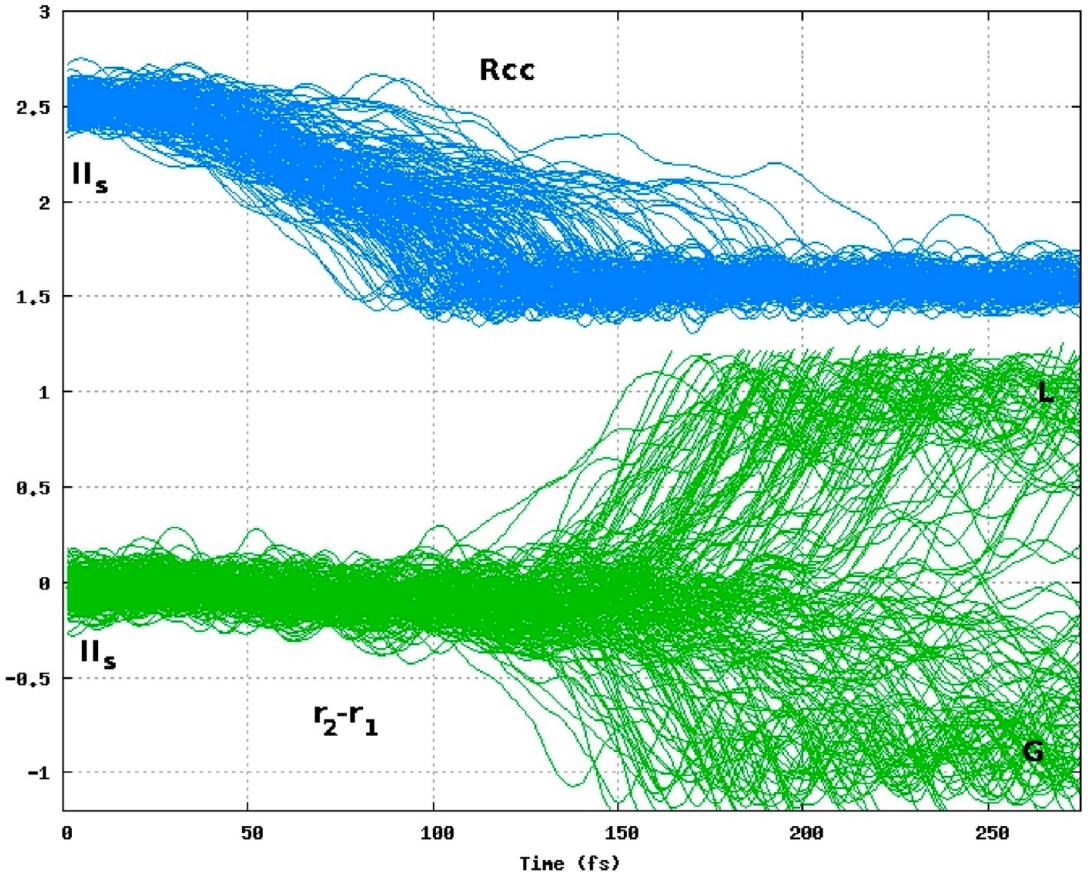

Figure 8. Trajectories relevant to the rearrangement of cation $\mathbf{II}_s$ as functions of time. Blue lines, R_{CC}; green lines, $r_2 - r_1$.

separated by a ridge originating from **V**. The topology of this case seems to differ from that found by other authors, where the key point is a valley bifurcation leading to two minima on the PES.[12]

The structural reasons explain the *memory effect*, but the occurrence of the *leakage* has not yet been covered. At first sight, the *leakage* could be the explained by the interconversion of cations **G** and **L** through **V**. However, as reported above, the solvolyses of **VII′** and **VII″** exclude this possibility, so the *leakage* must take place in a different way. As we can see on the right side of Figure 2, in the initial phase of the rearrangements, $r_2 - r_1$ (and therefore r_1 and r_2) changes by only a small amount until R_{CC} gets below 1.8−1.9 Å. Therefore, it is possible that dynamics effects[12,13] could allow the two pathways to cross each other. This is just what we verified by calculations using a Born−Oppenheimer molecular dynamics model (see Computational Methods). The resulting trajectories are shown in two More O'Ferrall−Jencks diagrams: Figure 6 for the rearrangement originating from TS $\mathbf{II}_s$ and Figure 7 for the rearrangement originating from TS $\mathbf{II}_a$.

In Figure 6, we can see that about half of the trajectories from $\mathbf{II}_s$ lead to cation **L** instead of cation **G**. The **G**/**L** ratio is 1.0, and the excess of **G** is only 2%. By contrast, in Figure 7 we can see that a great majority of the trajectories from $\mathbf{II}_a$ go to the expected cation **L**, while only a few go to cation **G**. This corresponds to an **L**/**G** ratio of 27 and an excess of **L** of 96%. These values are in qualitative agreement with the experimental findings shown in Table 1): in the rearrangement that follows TS $\mathbf{II}_a$, the *memory effect* is more efficient (less *leakage*) than in the rearrangement that follows TS $\mathbf{II}_s$. The oscillation of the trajectories could also allow solvent capture, yielding the minor products and $\mathbf{III}_s$, $\mathbf{III}_a$, **VI′**, and **VI″**. Comparing Figures 6 and 7, we can observe that when the $\mathbf{C}^8$−$\mathbf{C}^4$ bond formation is almost complete (R_{CC} below 1.7 Å), the trajectories from TS $\mathbf{II}_s$ oscillate around **V** and its ridge (the gray line), while the trajectories from TS $\mathbf{II}_a$ definitely oscillate in the **L** region (above the ridge from **V**), determining the greater *leakage* in the rearrangement of $\mathbf{II}_s$. This behavior can also be observed in Figures 8 and 9, which report the values of R_{CC} and $r_2 - r_1$ as functions of the time. In the rearrangement that follows TS $\mathbf{II}_s$ we can see that the $\mathbf{C}^8$−$\mathbf{C}^4$ bond forms (R_{CC} oscillates around 1.5 Å) within 90 to 150 fs (Figure 8, blue lines). The evolution of $r_2 - r_1$ shows on the other hand that $\mathbf{C}^7$ starts to bend toward $\mathbf{C}^2$ or $\mathbf{C}^6$ only after 140 fs (Figure 8, green lines). By contrast, in the rearrangement that follows TS $\mathbf{II}_a$, we can see that while the $\mathbf{C}^8$−$\mathbf{C}^4$ bond also forms within 80−140 fs, $\mathbf{C}^7$ starts to bend toward $\mathbf{C}^2$ or $\mathbf{C}^6$ (Figure 9, green lines) already after 80 fs (Figure 9, red lines). Moreover, we can observe (green lines in Figures 8 and 9) that when **G** or **L** is formed (i.e., $|r_2 - r_1| > 0.5$ Å), the trajectories no longer cross the line $r_2 - r_1 = 0$ Å (i.e., **G** and **L** do not interconvert through **V**).

In both cases, the "*first rearrangement*" (formation of the $\mathbf{C}^8$−$\mathbf{C}^4$ bond) is complete within 150 fs, quite similar to other cases,[13,14] while the "*second rearrangement*" (formation of **G** or **L**) requires a longer time. A possible explanation for the different extents of *leakage* is that because the p/π orbital is more diffuse than the σ orbital, the interaction of incipient empty p orbital on $\mathbf{C}^7$ (particularly when the $\mathbf{C}^4$−$\mathbf{C}^8$ bond is already formed) with the former is more effective than the interaction with the latter (see Figure 4). Therefore, during the oscillation of the

dx.doi.org/10.1021/jo401188e | J. Org. Chem. 2013, 78, 9041−9050

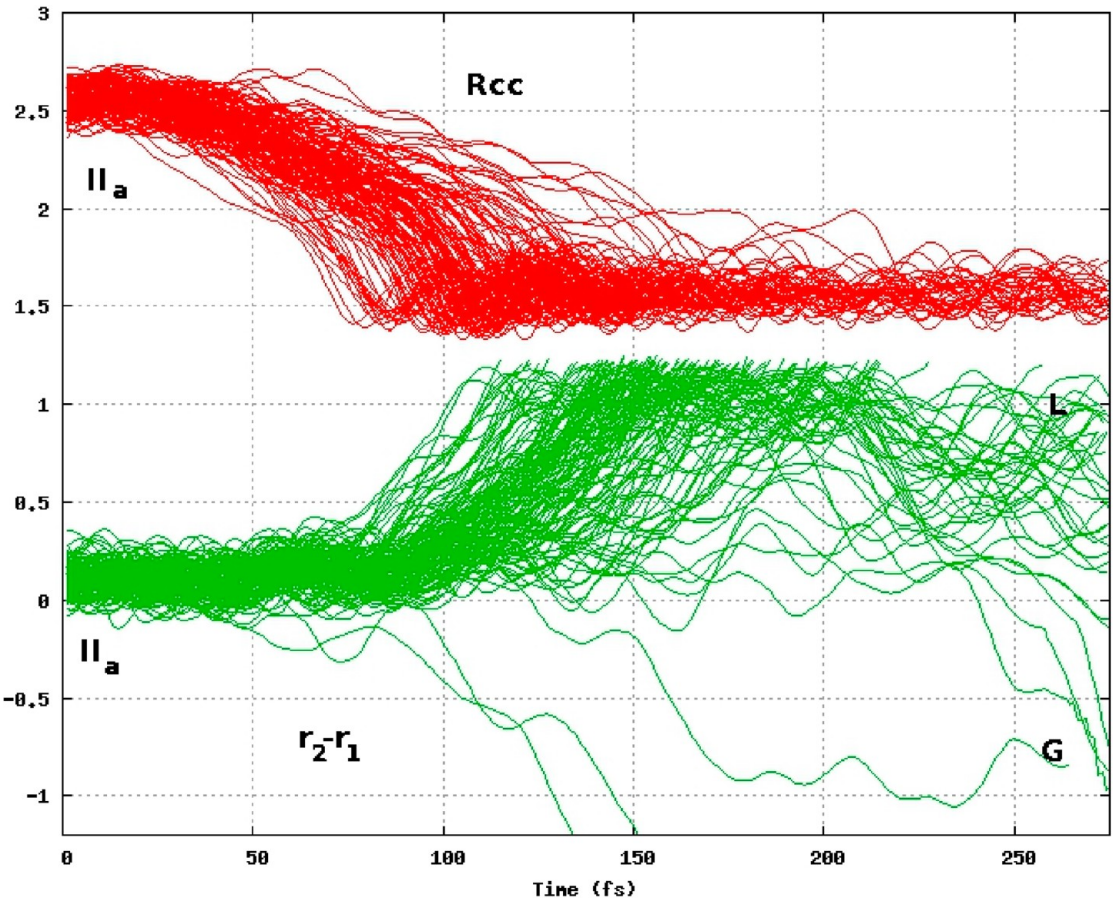

Figure 9. Trajectories relevant to the rearrangement of cation $\mathbf{II}_a$ as functions of time. Red lines, R_{CC}; green lines, $r_2 - r_1$.

trajectories beyond TS $\mathbf{II}_s$ along and in some proximity of the corresponding IRC pathway (black line in Figure 2) the interaction with the p/π orbital can in some cases prevail over the interaction with the σ orbital, leading the rearrangement toward cation **L** instead of **G** and thus giving rise to the *leakage*. In the rearrangement beyond TS $\mathbf{II}_a$, the interaction of the empty p orbital with the p/π orbital (leading to **L**) is further favored for structural reasons ($\mathbf{C}^7$ is closer to $\mathbf{C}^2$), so less *leakage* is observed.

CONCLUSIONS

The *memory effect* in the rearrangement of the two carbocations generated in the solvolysis of the *syn*- and *anti*-norborn-2-en-7-ylmethyl-**X** systems ($\mathbf{I}_s$ and $\mathbf{I}_a$) has been explained here as being determined by the different interactions that build up along the rearrangement pathways for the cationic systems. The parameter $r_2 - r_1$ determines which is the dominant stabilizing orbital interaction of the incipient empty p orbital on $\mathbf{C}^7$ (see Figure 4): that with the p/π orbital on $\mathbf{C}^2$ (which leads to cation **L**) or, alternatively, the one with the σ orbital of the $\mathbf{C}^1$–$\mathbf{C}^6$ bond (which leads instead to cation **G**). The study of the PES has shown that the carbocations $\mathbf{IV}_s$ and $\mathbf{IV}_a$ proposed in the literature (Scheme 3) do not exist as stationary points on the PES and that structure **V** is a TS connecting cations **G** and **L**. PES and dynamic studies (and experiments[5a] with **VII′** and **VII″**) showed that **V** has no role despite its low energy relative to cations **G** (17 kcal mol^{-1}) and **L** (10–15 kcal mol^{-1}). These energy barriers should lead products from cation **G** to prevail, but this would disagree with the experimental findings. Moreover, when dynamical effects are introduced, the oscillation of the rearrangement trajectories can overcome the initial structural guidance that is responsible for the *memory effect*, leading in some cases to the opposite result in the orbital interactions. This effect in turn partially yields the products not expected on the basis of the starting structure, thus giving rise to the *leakage* phenomenon (partial loss of the *memory effect*).

COMPUTATIONAL METHODS

The PES was first explored by optimizing geometries within density functional theory (DFT),[15] making use of the composite functionals B3LYP,[16] mPW1PW91,[17] and BB1K.[18] Several functionals have already been tested;[19] we chose B3LYP because it was the most used even in recent papers,[20] while mPW1PW91[19c−e,21] and BB1K[12a,19b] were suggested in the more recent papers. From inspection of Tables 2 and 3, we can observe a substantial agreement between the three functionals, which show the same qualitative mechanistic picture. The basis set used was Pople's 6-31G(d).[22] Solvent effects were introduced during geometry optimization using the polarized continuum method (PCM)[23] within the universal solvation model based on solute electron density (SMD).[24] All minima and TSs were fully characterized by vibrational analysis,[25] and the zero-point energies (ZPEs) combined with electronic energies (E_{el}) are reported in Tables 2 and 3. The nature of the TSs was confirmed by IRC optimizations.[26]

The dynamical study was performed within the Born–Oppenheimer molecular dynamics model.[27] The energies and gradients were calculated with the HF method[28] and the 3-21G basis set.[29] This level of theory satisfactorily reproduced the DFT surface (see Table 3 and compare Figures 1 and 2 in the Supporting Information) and allowed the calculation of an adequate number of trajectories. We calculated a total of 500 trajectories (250 from TS $\mathbf{II}_s$ and 250 from TS $\mathbf{II}_a$).

dx.doi.org/10.1021/jo401188e | J. Org. Chem. 2013, 78, 9041–9050

All of the calculations were performed using Gaussian 09 software.[30] Figures 1 and 3 and Figures 1 and 2 in the Supporting Information were obtained using the program Molden.[31]

■ ASSOCIATED CONTENT

Supporting Information

Cartesian coordinates of all structures, their absolute energies in hartrees and energy differences in kcal/mol, and energy profiles for the IRCs. This material is available free of charge via the Internet at http://pubs.acs.org.

■ AUTHOR INFORMATION

Corresponding Author

*E-mail: giovanni.ghigo@unito.it.

Notes

The authors declare no competing financial interest.

■ ACKNOWLEDGMENTS

Local funding from Torino University is gratefully acknowledged.

■ REFERENCES

(1) Berson, J. A. *Angew. Chem., Int. Ed. Engl.* **1968**, *7*, 779−791.

(2) Smith, M. J.; March, J. *March's Advanced Organic Chemistry*, 6th ed.; Wiley: Hoboken, NJ, 2007; Chapter 10, pp 446−468.

(3) Silver, M. *J. Am. Chem. Soc.* **1961**, *83*, 3482−3486.

(4) (a) Berson, J. A.; Reynolds-Warnhoff, P. *J. Am. Chem. Soc.* **1962**, *84*, 682−684. (b) Berson, J. A.; Willner, D. *J. Am. Chem. Soc.* **1962**, *84*, 675−676.

(5) (a) Berson, J. A.; Gajewski, J. J. *J. Am. Chem. Soc.* **1964**, *86*, 5020−5021. (b) Berson, J. A.; Reynolds-Warnhoff, P. *J. Am. Chem. Soc.* **1964**, *86*, 595−609. (c) Berson, J. A.; Willner, D. *J. Am. Chem. Soc.* **1964**, *86*, 609−616. (d) Berson, J. A.; Gajewski, J. J.; Donald, D. S. *J. Am. Chem. Soc.* **1969**, *91*, 5550−5566. (e) Berson, J. A.; Poonian, M. S.; Libbey, W. J. *J. Am. Chem. Soc.* **1969**, *91*, 5567−5579. (f) Berson, J. A.; Donald, D. S.; Libbey, W. J. *J. Am. Chem. Soc.* **1969**, *91*, 5580−5593. (g) Berson, J. A.; Wege, D.; Clarke, G. M.; Bergman, R. G. *J. Am. Chem. Soc.* **1969**, *91*, 5594−5600. (h) Berson, J. A.; Luibrand, R. T.; Kundu, N. G.; Morris, D. G. *J. Am. Chem. Soc.* **1971**, *93*, 3075−3077.

(6) (a) Collins, C. J. *Acc. Chem. Res.* **1971**, *4*, 315−322. (b) Collins, C. J.; Glover, I. T.; Eckart, M. D.; Raeen, V. F.; Benjamin, B. M.; Benjaminov, B. S. *J. Am. Chem. Soc.* **1972**, *94*, 899−908. (c) Collins, C. J. *Chem. Soc. Rev.* **1975**, *4*, 251−262.

(7) Smith, M. J.; March, J. *March's Advanced Organic Chemistry*, 6th ed.; Wiley: Hoboken, NJ, 2007; Chapter 18, pp 1570−1572.

(8) (a) Goering, H. L.; Sloan, M. F. *J. Am. Chem. Soc.* **1961**, *83*, 1992−1999. (b) Goering, H. L.; Greiner, R. W.; Sloan, M. F. *J. Am. Chem. Soc.* **1961**, *83*, 1391−1397. (c) Goering, H. L.; Towns, D. L. *J. Am. Chem. Soc.* **1963**, *85*, 2295−2298.

(9) (a) LeBel, N. A.; Huber, J. E. *J. Am. Chem. Soc.* **1963**, *85*, 3193−3199. (b) Fraser, R. R.; O'Farrell, S. *Tetrahedron Lett.* **1962**, *3*, 1143−1146.

(10) Tests performed with other leaving groups (bromide and nosylate) showed very high and unrealistic barriers possibly because of the lack of explicit solvent molecules.

(11) (a) Tantillo, J. D. *J. Phys. Org. Chem.* **2008**, *21*, 561−570. (b) Williams, A. *Concerted Organic and Bio-Organic Mechanisms*; CRC Press: Boca Raton, FL, 2000. (c) Dewar, M. J. S. *J. Am. Chem. Soc.* **1984**, *106*, 209−219. (d) Hess, B. A.; Smentek, L. *Org. Biomol. Chem.* **2012**, *10*, 7503−7509. (e) Tantillo, J. D. *Nat. Prod. Rep.* **2011**, *28*, 1035−1053.

(12) (a) Siebert, M. R.; Zhang, J.; Addepalli, S. V.; Tantillo, D. J.; Hase, W. L. *J. Am. Chem. Soc.* **2011**, *133*, 8335−8343. (b) Siebert, M. R.; Manikandan, P.; Sun, R.; Tantillo, D. J.; Hase, W. L. *J. Chem. Theory Comput.* **2012**, *8*, 1212−1222. (c) Rehbein, J.; Carpenter, B. K. *Phys. Chem. Chem. Phys.* **2011**, *13*, 20906−20922.

(13) Black, K.; Liu, P.; Xu, L.; Doubleday, C.; Houk, K. N. *Proc. Natl. Acad. Sci. U.S.A.* **2012**, *109*, 12860−12865.

(14) Ammal, S. C.; Yamataka, H.; Aida, M.; Dupuis, M. *Science* **2003**, *299*, 1555−1557.

(15) (a) Parr, R. G.; Yang, W. *Density Functional Theory of Atoms and Molecules*; Oxford University Press: New York, 1989. (b) Jensen, W. *Introduction to Computational Chemistry*; Wiley; Chichester, U.K., 1999; Chapter 6.

(16) (a) Becke, A. D. *J. Chem. Phys.* **1993**, *98*, 5648−5652. (b) Koch, W.; Holthausen, M. C. *A Chemist's Guide to Density Functional Theory*; Wiley-VCH: Weinheim, Germany, 2000; Chapter 6. (c) Becke, A. D. *Phys. Rev. A* **1988**, *38*, 3098−3100. (d) Lee, C.; Yang, W.; Parr, R. G. *Phys. Rev. B* **1988**, *37*, 785−789.

(17) (a) Adamo, C.; Barone, V. *J. Chem. Phys.* **1998**, *108*, 664−675. (b) Perdew, J. P. In *Electronic Structure of Solids '91*; Ziesche, P., Eschrig, H., Eds.; Akademie Verlag: Berlin, 1991; pp 11−20.

(18) Zhao, Y.; Lynch, B. J.; Truhlar, D. G. *J. Phys. Chem. A* **2004**, *108*, 2715−2719.

(19) For example, see: (a) Mackie, I. D.; Govindhakannan, J.; DiLabio, G. A. *J. Phys. Chem. A* **2008**, *112*, 4004−4010. (b) Weitman, M.; Major, D. T. *J. Am. Chem. Soc.* **2010**, *132*, 6349−6360. (c) Matsuda, S. P. T.; Wilson, W. K.; Xiong, Q. *Org. Biomol. Chem.* **2006**, *4*, 530−543. (d) Hong, Y. J.; Tantillo, D. J. *Org. Biomol. Chem.* **2010**, *8*, 4589−4600. (e) Hong, Y. J.; Tantillo, D. J. *Nat. Chem.* **2009**, *1*, 384−389. (f) Barquera-Lozada, J. E.; Cuevas, G. *J. Org. Chem.* **2009**, *74*, 874−883.

(20) (a) Nguyen, Q. N. N.; Tantillo, D. J. *Beilstein J. Org. Chem.* **2013**, *9*, 323−331. (b) Tantillo, D. J.; Schleyer, P. v. R. *Org. Lett.* **2013**, *15*, 1725−1727.

(21) (a) Smentek, L.; Hess, B. A., Jr. *J. Am. Chem. Soc.* **2010**, *132*, 17111−17117. (b) Hong, Y. J.; Tantillo, D. J. *Chem. Sci.* **2010**, *1*, 609−614.

(22) (a) Hehre, W. J.; Ditchfield, R.; Pople, J. A. *J. Chem. Phys.* **1972**, *56*, 2257−2261. (b) Hariharan, P. C.; Pople, J. A. *Theor. Chim. Acta* **1973**, *28*, 213−222. (c) Clark, T.; Chandrasekhar, J.; Schleyer, P. v. R. *J. Comput. Chem.* **1983**, *4*, 294−301. (d) Frisch, M. J.; Pople, J. A.; Binkley, J. S. *J. Chem. Phys.* **1984**, *80*, 3265−3269.

(23) (a) Barone, V.; Cossi, M. *J. Phys. Chem. A* **1998**, *102*, 1995−2001. (b) Cossi, M.; Rega, N.; Scalmani, G.; Barone, V. *J. Chem. Phys.* **2001**, *114*, 5691−5701. (c) Cancès, M. T.; Mennucci, B.; Tomasi, J. *J. Chem. Phys.* **1997**, *107*, 3032−3041. (d) Cossi, M.; Barone, V.; Mennucci, B.; Tomasi, J. *Chem. Phys. Lett.* **1998**, *286*, 253−260. (e) Mennucci, B.; Tomasi, J. *J. Chem. Phys.* **1997**, *106*, 5151−5158.

(24) (a) Marenich, A. V.; Cramer, C. J.; Truhlar, D. G. *J. Phys. Chem. B* **2009**, *113*, 6378−6396. (b) Marenich, A. V.; Cramer, C. J.; Truhlar, D. G. *J. Phys. Chem. B* **2009**, *113*, 4538−4543.

(25) Reaction enthalpies and free energies were computed as outlined, for instance, in: Foresman, J. B.; Frisch, Æ. *Exploring Chemistry with Electronic Structure Methods*; Gaussian, Inc.: Pittsburgh, PA, **1996**, pp 166−168.

(26) (a) Gonzalez, C.; Schlegel, H. B. *J. Chem. Phys.* **1989**, *90*, 2154−2161. (b) Gonzalez, C.; Schlegel, H. B. *J. Phys. Chem.* **1990**, *94*, 5523−5527 and references therein.

(27) (a) Helgaker, T.; Uggerud, E.; Jensen, H. J. A. *Chem. Phys. Lett.* **1990**, *173*, 145−150. (b) Uggerud, E.; Helgaker, T. *J. Am. Chem. Soc.* **1992**, *114*, 4265−4268. (c) Chen, W.; Hase, W. L.; Schlegel, H. B. *Chem. Phys. Lett.* **1994**, *228*, 436−442. (d) Millam, J. M.; Bakken, V.; Chen, W.; Hase, W. L.; Schlegel, H. B. *J. Chem. Phys.* **1999**, *111*, 3800−3805. (e) Li, X.; Millam, J. M.; Schlegel, H. B. *J. Chem. Phys.* **2000**, *113*, 10062−10067.

(28) (a) Roothan, C. C. J. *Rev. Mod. Phys.* **1951**, *23*, 69−76. (b) Pople, J. A.; Nesbet, R. K. *J. Chem. Phys.* **1954**, *22*, 571−572. (c) Szabo, A.; Ostlund, N. S. *Modern Quantum Chemistry*; McGraw-Hill: New York, 1982; Chapter 3.

(29) Binkley, J. S.; Pople, J. A.; Hehre, W. J. *J. Am. Chem. Soc.* **1980**, *102*, 939−947.

(30) Frisch, M. J.; Trucks, G. W.; Schlegel, H. B.; Scuseria, G. E.; Robb, M. A.; Cheeseman, J. R.; Scalmani, G.; Barone, V.; Mennucci, B.; Petersson, G. A.; Nakatsuji, H.; Caricato, M.; Li, X.; Hratchian, H.

P.; Izmaylov, A. F.; Bloino, J.; Zheng, G.; Sonnenberg, J. L.; Hada, M.; Ehara, M.; Toyota, K.; Fukuda, R.; Hasegawa, J.; Ishida, M.; Nakajima, T.; Honda, Y.; Kitao, O.; Nakai, H.; Vreven, T.; Montgomery, J. A., Jr.; Peralta, J. E.; Ogliaro, F.; Bearpark, M.; Heyd, J. J.; Brothers, E.; Kudin, K. N.; Staroverov, V. N.; Kobayashi, R.; Normand, J.; Raghavachari, K.; Rendell, A.; Burant, J. C.; Iyengar, S. S.; Tomasi, J.; Cossi, M.; Rega, N.; Millam, N. J.; Klene, M.; Knox, J. E.; Cross, J. B.; Bakken, V.; Adamo, C.; Jaramillo, J.; Gomperts, R.; Stratmann, R. E.; Yazyev, O.; Austin, A. J.; Cammi, R.; Pomelli, C.; Ochterski, J. W.; Martin, R. L.; Morokuma, K.; Zakrzewski, V. G.; Voth, G. A.; Salvador, P.; Dannenberg, J. J.; Dapprich, S.; Daniels, A. D.; Farkas, Ö.; Foresman, J. B.; Ortiz, J. V.; Cioslowski, J.; Fox, D. J. *Gaussian 09*, revision A.1; Gaussian, Inc., Wallingford, CT, 2009.

(31) Schaftenaar, G.; Noordik, J. H. Molden: A pre- and post-processing program for molecular and electronic structures. *J. Comput.-Aided Mol. Des.* **2000**, *14*, 123−134.